Fabrication and characterization of poly(fullerene) thin films for gas sensors

André Vs Simõis, Marcelo Borro, Maria Ers Medina, Luiz Riga, Nyara Ferreira, Pedro Silva, Hasina H. Ramanitra, Meera Stephen, Nara Souza, Roger C. Hiorns, et al.

FABRICATION AND CHARACTERIZATION OF POLY(FULLERENE) THIN FILMS FOR GAS SENSORS

André V. S. Simõis[1]*, Marcelo S. Borro[1], Maria E. R. S. Medina[1], Luiz A. Riga Junior[1], Nyara D. Ferreira[1], Pedro L. Silva[1], Hasina H. Ramanitra[2], Meera Stephen[2], Nara C. Souza[3], Roger C. Hiorns[2], Deuber L. S. Agostini[1], Clarissa A. Olivati [1]

[1] São Paulo State University (Unesp), School of Technology and Sciences, Presidente Prudente - SP, Brazil.

[2] CNRS/Univ Pau & Pays Adour, Institut des Science Analytiques et Physico-Chimie pour l'Environnement et les Materiaux, UMR5254, 64000, Pau, France.

[3] Laboratório de Nanosistemas e Tecnologias, LabNano, Universidade Federal de Goiás, Ap. de Goiânia, Goiás, Brazil

***Corresponding author: andre.simois@unesp.br**

ABSTRACT

Ammonia, despite being a naturally generated compound in the metabolic process, can be harmful to health in higher concentrations. In this context, sensor devices are directly related to health and safety measurements to detect the presence of such substances. In this work, we study materials derived from fullerene, a material with a high electron affinity. We characterize three fullerene derivatives, namely PCBM, OPCBMMB and PPCBMB, and verify their applicability as ammonia sensors. The materials were studied in the form of thin films, produced by Langmuir–Schaefer and drop-casting techniques. Optical characterization was performed using UV–visible spectroscopy while morphological characteristics were studied using atomic force microscopy (AFM) and optical microscopy (OM). Current versus voltage and current versus time measurements were performed in order to determine the films' conductivities, electrical resistances

and gas-sensing properties. UV–visible absorption was observed at lower wavelengths, with peaks in the UV region. In the electrical measurements, differences were observed between the deposition techniques, with the Langmuir–Schaefer films showing a higher conductivity than the drop-casting films. AFM and OM also showed differences in the film surfaces between the techniques, with a rougher surface on the drop- casting films. When exposed to ammonia, the materials showed electrical responses at every cycle, with a significant increase in their electrical responses.

1. INTRODUCTION

Fullerene was discovered in 1985 by H. W. Kroto *et al*., who was conducting experiments aimed at unraveling the mechanism of nucleation of carbon atoms, observed in red giant stars [1]. Instead, the result obtained was a series of carbon clusters, with varying amounts of the atom, but with the highest concentration and structural stability observed at 60 carbons. The structure of these molecule consists of a truncated icosahedron, a polygon with 60 vertices where the carbon atoms are located, and has 32 faces, of which 12 are pentagonal and 20 are hexagonal, which makes the molecule highly symmetrical [1]–[3]. The so-called [6,6]-bonds between the rings of hexagons have aspects of π-bonds, while the [5,6] single bonds reside mainly at the pentagons. The main reactions of fullerene occur at the π-bonds, as seen in Figure 1 [4].

Figure 1. Face-on view of the structure of fullerene (C_{60}).

As a consequence of a great chemical and structural stability, fullerene is considered as the third allotrope of carbon, after diamond and graphite [2]. Phenyl-C_{61}-butyric acid

methyl ester (PCBM) stands out as one of the most common fullerene derivatives used in the field of organic electronics, due to its enhanced solubility in organic solvents by way its modification with a sidechain which breaks some of the C_{60} symmetries. Fullerene and PCBM's exhibit exceptional strong electron affinity, which gives these molecules importance for organic electronics, optoelectronics and photovoltaics. Importantly, for this work, their electrophilicity means that they are particularly sensitive to the rich electronic characteristics of molecules containing nitrogen atoms, which have lone pairs of electrons that can interact with the fullerene. Evidence for this can be given by th example of the first known reactions involving fullerene with an amine [5].

Exploiting the properties of fullerenes has been improved by using derivatives such as PCBM, however, a constant problem remains their strong tendency to form aggregates in an uncontrolled manner. This means that it difficult to explore their properties and applications, since there is little or even no control over its aggregations [6]. One way to get around this is to incorporate fullerene into a polymeric structure, which means that its aggregation becomes more controlled, its solubility is improved in many solvents, such as chloroform, used in this work, and it becomes a more malleable and easier to manipulate material. This process can be done through several chemical procedures, to highlight here ATRAP (atom transfer radical addition polymerization) and SACAP (sterically controlled azomethine ylide cycloaddition polymerization techniques, through which Ramanitra *et al*. [7] and Stephen *at al.* [8] showed it was possible to incorporate PCBM into polymer main chains. Both techniques show consistent and high-yield results in the production of oligo(fullerene)s and poly(fullerene)s, respectively.

One of the methods for the deposition of conductive polymers is the Langmuir technique, known to produce films with an oriented molecular structure when used with amphiphilic molecules [9], [10]. The technique consists of transferring the Langmuir films formed at the air/water interface to a solid substrate in a Langmuir trough. For the formation of Langmuir films, the solution containing the material is spread on the surface of the subphase, the solvent evaporates, and the remaining molecules are compressed by mobile barriers, causing them to gradually approach, characterizing a surface pressure isotherm, to eventually form a monolayer with a high level of organization [11]. Langmuir techniques can be divided into two types according to the way in which the film is transferred from the subphase to the substrate. A horizontal transfer, performed by pressing a substrate horizontally against the surface layer and more commonly used for

more rigid monolayers, is called Langmuir-Schaefer (LS) [12], and the vertical transfer controlled by software, through immersion and emersion of the substrate in the subphase, is called Langmuir-Blodgett (LB). In both techniques, the process can be repeated to transfer multiple layers to the substrate.

A gas sensor is a device that receives stimulus from an analyte present in the atmosphere and generates an electrical response. This effect may be due to adsorption, which is a process of gas molecule adhesion on the surface of a solid film, or absorption, where ions, molecules, and atoms are incorporated into the volume of the material [13], [14]. Sensor devices are widely used in industry [15]–[17], such as in the quality control process of metals [18] and in the detection of toxic substances, acting as safety devices. Ammonia is an important part of the atmosphere and acts as a neutralizer of generated gases, such as carbon dioxide [19]. However, when in high concentrations, ammonia is a toxic gas that can seriously affect the respiratory system, potentially causing serious consequences for the individual [20].

One of the main limitations found on studies about gas sensors is the temperature of operation of these devices. Most of the sensors studied today are produced from metal oxides, that require a higher temperature to operate and recover properly from the analyte's effects [21], [22].

In recent years, research in gas sensors area has been pointing the use of organic and polymeric materials as a viable way to overcome this limitation, because of the room temperature operation of the organic materials and their reactivity, which makes easier to manipulate these materials to achieve an organic sensor with higher conductivity [23], [24]. In addition, polymer-based materials are expected to be much easier to cast to give different forms and surfaces, to be energetically economic as they do not require sintering or similar high temperature processes, and can be cast using common organic solvents.

In this context, the central objective is to study thin films fabricated using fullerene materials, deposited by Langmuir-Schaeffer and drop-cast techniques. The thin films were characterized by electrical, optical and morphological measurements, and applied as an active layer for ammonia sensor devices.

2. EXPERIMENTAL SECTION

2.1 – Materials

In this work, three fullerene based materials were studied, namely PCBM, oligo{(phenyl-C_{61}-butyric acid methyl ester)-*alt*-[1,4-bis(bromomethyl)-2,5-bis(octyloxy)benzene]} (OPCBMMB) and poly{[bispyrrolidino(phenyl-C_{61}-butyric acid methyl ester)-*alt*-[2,5-bis(octyloxy)benzene]} (PPCBMB). Figure 2 represents the chemical structures of the studied materials.

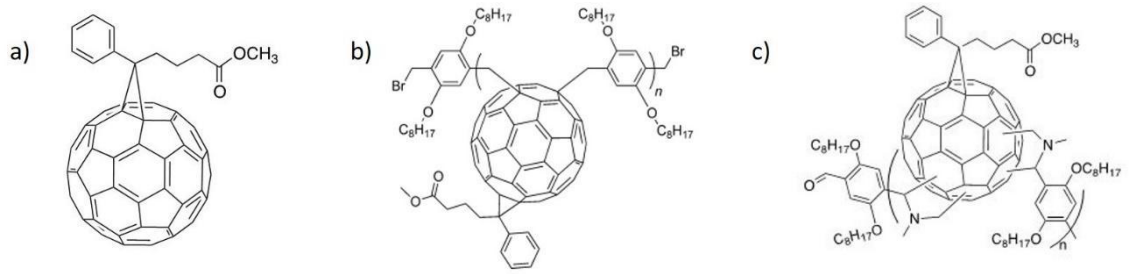

Figure 2. Chemical structures of **a)** PCBM; **b)** OPCBMMB; **c)** PPCBMB

PCBM was commercially obtained by Sigma Aldrich, while OPCBMMB was prepared as detailed by Ramanitra *et al* [7] and PPCBMB was prepared as indicated by Stephen *et al*. [8], the samples having the exact same characteristics as detailed in those papers. We give a brief summary of their preparations here. OPCBMMB was made using the aforementioned ATRAP method, in which a bifunctional dibromethylated comonomer (1,4-bis(bromomethyl)-2,5-bis(octyloxy)benzene) was mixed with CuBr, bipyridine and PCBM in toluene at 100 ˚C for 16h. The CuBr, transported by the bipyridine in the toluene generates methylene radicals on the comonomer which subsequently react with the PCBM to generate an oligomer. The product was found to have a relatively low molecular weight, with a distribution of between one and four repeating units. Indeed, around 35% of the material was unreacted PCBM. In the case of the PPCBMB, a much higher molecular weight was attained by using the so-called SACAP method. Here, the PCBM was reacted with a 2,5-bis(octyloxy)terephthalaldehyde and presence of *N*-methylglycine in refluxing toluene to deliver a polymer with molecular weights estimated to be of the order of $M_n \approx 24\ 600$ g mol^{-1} and $M_w \approx 73\ 800$ g mol^{-1}. All the materials were studied from chloroform-cast solutions, in which they all display reasonably good solubility.

For optical and morphological characterizations, solid substrates were deposited on glass slides. For electrical characterizations in direct current and sensory measurements, glass slides with interdigitated gold electrodes (IDE/Au) with 50 digits. Each digit is 110 nm in height, 8 mm in length and 100 μm wide. The spacing between each digit is 100 μm.

The utilization of these IDEs was required for this work, because in each pair of digits, the total current is amplified [25], which facilitates the process of electrical characterization in materials with the low electrical conductivity of undoped semiconductors such as fullerenes.

2.2 – Drop Casting Films

The drop casting technique is one of the simplest film deposition techniques from solution [26]. In this method, the solution is dripped onto a horizontal substrate with the aid of an electronic pipette. Then the solvent evaporates, so that the film remains on the substrate due to Van der Waals forces [27].

The drop casting technique, however, does not allow for control over the film formation, facilitating the formation of agglomerates in the structure, which results in films with a heterogeneous surface. The lack of control over the film formation also limits the control over the film thickness. Factors such as deposited volume and solution concentration can help regulate the final film thickness, but with a low accuracy [26]–[28].

For the deposition of the drop casting films, a volume of 0.2 mL of the solutions, at a concentration of 1.0 mg mL^{-1}, was dipped onto the substrate with the aid of an electronic micropipette. The films quickly and visibly dried at room temperature and were considered dry after 30 minutes leaving the thin film on the substrate.

Solvent evaporation is one of the most important parts of the process, where we have the choice to let it evaporate naturally or use thermal process to accelerate the process, however, disturbing the system can impact detrimentally on film morphology [29], [30].

2.3 – Langmuir Films Fabrication and Deposition

In general, Langmuir films are defined as a monolayer film, with a monomolecular thickness, formed by the compression of amphiphilic molecules on an aqueous subphase. Among the advantages of the Langmuir deposition techniques, we can highlight the precise control of the film thickness, the achievement of nanostructured films, with high structural order and molecular orientation controlled by amphiphilic interactions with the subphase.

To the study of the isotherm, that allow us to observe the film formation, 250 μL of the solution (0.2 mg mL^{-1}), using chloroform as solvent, was spread over the aqueous subphase on the Langmuir through. For the film deposition, the spread volume was higher (500 μL) in order to ensure that there is enough material on the subphase to transfer 25 layers onto the substrate via the LS technique.

After spreading the solution, the solvent evaporates, leaving only the spread material present in the subphase. The barriers then begin to close slowly at a rate of 10 mm min^{-1}, starting the compression process. This compression causes the molecules present in the subphase to move closer to each other, until they begin intermolecular interactions, which characterizes a surface-pressure isotherm ($\pi - A$), where variations in the pressure causes changes on the behavior of complex amphiphilic molecules, such as reorientation and conformal transformations [31]. With the isotherms, we analyze the mean molecular area occupied by the studied materials for different values of surface pressure.

2.4 – Optical Microscopy and AFM

The morphology of the films was analyzed by optical microscopy (*Nikon Eclipse Ci / L, Tokyo, Japan*). Images of atomic force microscopy (*EasyScan II, Nanosurf, Liestal, Switzerland*) in an intermittent mode (512 × 512 pixels) were acquired in a scan window of 30 × 30 μm, under ambient conditions at room temperature. The tapping mode was selected, instead of the contact mode, since it is less damaging to the surfaces under investigation [32]. Root mean-square (RMS) roughness of films was determined using the *Nanosurf Instruments* software. At least five measures were taken and the errors were

the standard deviations. The technique provides the topography of a given surface and is used in the evaluation of defects and agglomerates, in addition to surface roughness calculations.

2.5 – UV-visible absorption spectra

By studying the processes of electronic transitions that take place within the ultraviolet-visible range, we can obtain important information about the molecule, regarding the absorption in this spectrum, as well as monitoring and verifying the growth of the films produced by Langmuir-Schaefer technique. It is also possible to get information about the internal structural organization of the films.

The UV-vis spectroscopy measurements took place in the incidence of light in the range of 900 to 300 nm. A detector located behind the sample is responsible for measuring the intensity of the light absorbed by the film. Lower wavelengths were avoided due to glass opacity for ultraviolet light.

2.6 – Electrical characterization in DC current

Current versus Voltage (*I versus V*) measurements were performed on a Keithley Semiconductor Parameter Analyzer mod. 238, over the range from – 15 to 15 V in steps of 0.5 V.

To calculate the electrical conductivity and resistance, Ohm's law equations were used, where the cell constant, for the interdigitated electrode used, has a value of 5.1 m^{-1}, as defined in previous works of the group, following Olthuis' method [33]–[35].

2.7 – Ammonia Sensors

To analyze the performance of these films as ammonia sensors, the electrical characterization of films through current *versus* time (*I versus t*) measurements were

performed. Initially, the films were flushed with nitrogen for 10 minutes to obtain an inert baseline, which cannot be guaranteed with air baseline. Following this, and throughout the whole process, the samples were subjected to a constant voltage of 5 V.

The measurements took place over 10 minutes cycles, alternating between the N_2 baseline and the NH_3 atmosphere, both in a saturation regime, which was carried into the sample by the N_2 flow (60 NL h^{-1}) through the home-made apparatus, internally measuring approximately 5.5 cm of radius by 7.0 cm of height. The cycles were repeated in order to verify the reproducibility of the obtained results.

To create the NH_3 saturated atmosphere, ammonium hydroxide was placed in a bubbler, where the nitrogen flow is responsible for carrying the ammonia vapors released to the sample.

3. RESULTS AND DISCUSSIONS

3.1 – Langmuir Films

In the study of surface pressure isotherms (π-A), it is possible to extract information about the studied materials during the film formation. It is possible to obtain data about the mean molecular area occupied by the materials in the Langmuir through, and the ideal pressure value required for deposition of Langmuir-Schaefer thin films. Figure 3 shows the results obtained from Surface pressure *vs* mean molecular area isotherms.

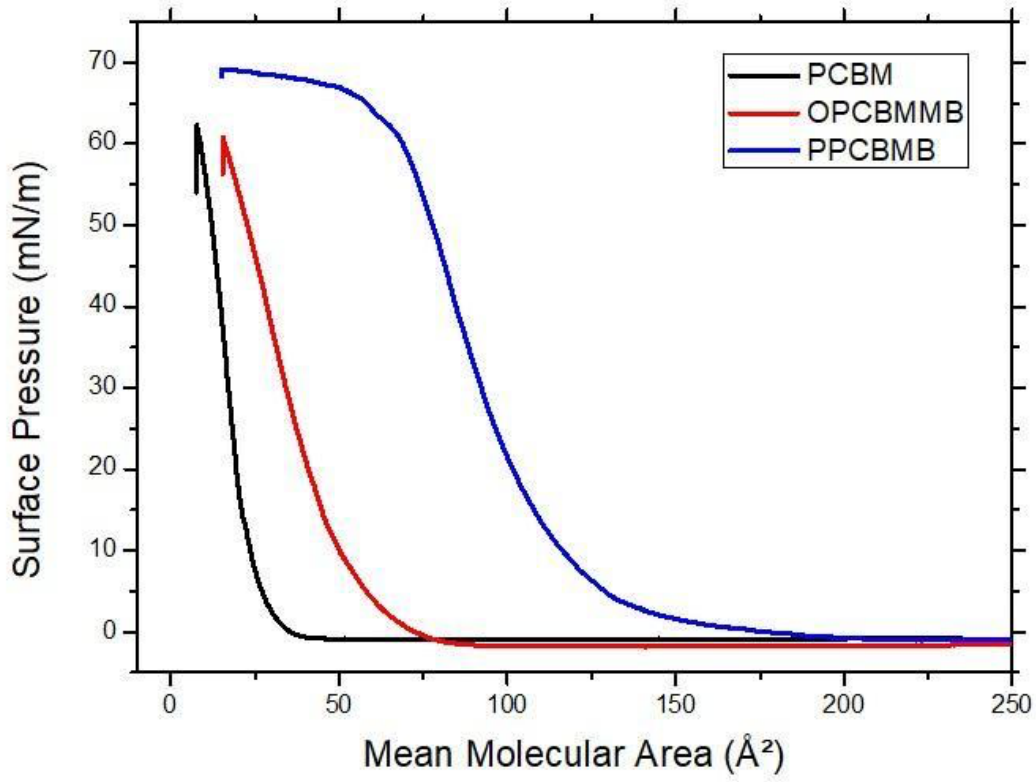

Figure 3. Surface pressure isotherms for PCBM (black), OPCBMMB (red) and PPCBMB (blue).

Analyzing the isotherms curves, it is possible to observe the absence of a well-defined transition phase, between a gas phase and a solid phase. It is also possible to note a linear region with a high compressibility, a characteristic feature of amphiphilic molecules [36]. These curves resemble condensed-liquid isotherms, according to Harkins classification [9].

It is also possible to estimate the mean molecular area the material occupies in the aqueous subphase, extrapolating the linear region in Figure 3, corresponding to the condensed phase of the isotherm. The values obtained for the mean molecular areas are given in Table 1.

Table 1. Mean molecular area of PCBM, OPCBMMB and PPCBMB

	Mean Molecular Area (Å^2)
PCBM	23.6
OPCBMMB	54.4
PPCBMB	116.4

Due to the presence of strong interactions between the π-bonds and the absence of hydrophilic groups, fullerenes tend to show uncontrolled aggregation on the aqueous subphase surface [37]–[39]. The integration of the PCBM into polymeric structures can reduce the aggregation by separating the spheres with comonomers. Importantly, large comonomers, with long alkyl chains can improve this situation. However, an additional possibility remains functionalizing fullerene with polar groups, such as hydroxyls, granting it an amphiphilic character [37], [38]. Functionalizing a material shows different results with respect to the control over the aggregation. In Table 1, we see that PCBM presents the lowest mean molecular area, followed by OPCBMMB and PPCBMB, with the last showing the highest value obtained airing from the differences in their structures. This can indeed result from the comonomers pushing fullerenes apart, but the impact of ethoxy groups on the comonomers, in addition to the methoxy groups on the PCBM cannot be ignored.

These results can indicate that the aggregation control was more effective in the polymer and the oligomer, due to their functionalization, with PCBM showing more aggregates on the aqueous subphase when compared to the other materials. In addition, Figure 4 brings a possible molecular organization of the materials in the aqueous subphase, similar to that found in previous works [40].

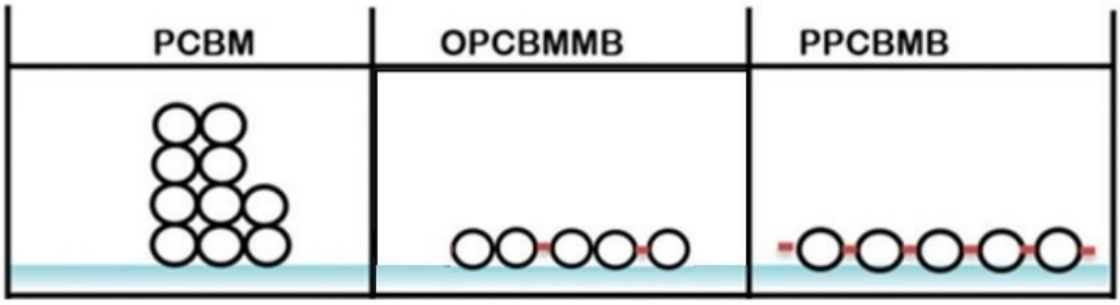

Figure 4. Proposed structures for molecular organization in the aqueous subphase. Adapted from [40].

With the isotherms, it is also possible to observe a well-defined condensed phase, represented by the linear region of high compression, that defines the ideal state for the film deposition into a solid substrate, with the Langmuir-Schaefer technique, without collapsing the monolayer [41]. In this way, we can determine the surface pressure of 20 mN m^{-1} as a favorable pressure for all the films deposition. For the LS films fabrication, 25 layers were deposited [42], [43].

3.2 – AFM and Optical Microscopy

Figure 5 presents the topographical images obtained by AFM for PCBM, OPCBMMB and PPCBMB, deposited by both Langmuir-Schaefer and drop-cast techniques.

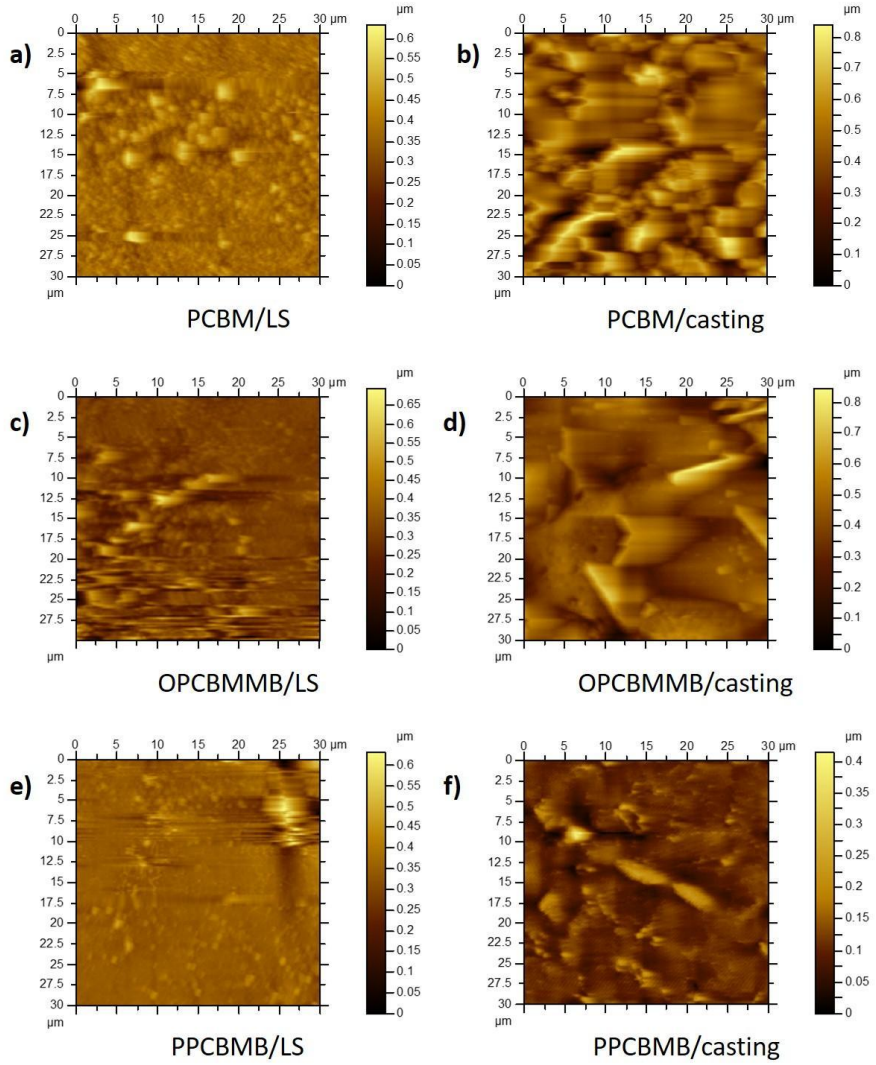

Figure 5. AFM images of the thin films **a)** PCBM/LS; **b)** PCBM/casting; **c)** OPCBMMB/LS; **d) O**PCBMMB/casting; **e)** PPCBMB/LS; **f)** PPCBMB/casting

On these images we can observe the presence of larger aggregates on the surface of the drop-cast films, that present a rougher surface when compared to the LS films, resulting from the intrinsic characteristic of the techniques used in the deposition. In the Langmuir films, we also observe that the surface roughness resulted in similar values, a fact that is not observed in the drop casting films, where PCBM resulted in a higher roughness value when compared to the polymer and the oligomer, as seen in Table 2.

This suggests that the functionalization applied during the synthetic processing of OPCBMMB and PPCBMB are capable of inhibiting the strong tendency of PCBM to form aggregates in an uncontrolled manner, which helps OPCBMMB and PPCBMB to

form films with a more homogeneous surface than PCBM, as can be seen in Figure 6, that shows images of the drop casting and LS films, obtained by optical microscopy, with a scale of 100 µm.

Table 2. Roughness (RMS) values obtained by AFM.

RMS (µm)	Langmuir-Schaefer	Drop-cast
PCBM	0.042	0.118
OPCBMMB	0.055	0.092
PPCBMB	0.039	0.029

This suggests that the functionalization applied during the synthetic processing of OPCBMMB and PPCBMB are capable of inhibiting the strong tendency of PCBM to form aggregates in an uncontrolled manner, which helps OPCBMMB and PPCBMB to form films with a more homogeneous surface than PCBM, as can be seen in Figure 6, that shows images of the drop casting and LS films, obtained by optical microscopy, with a scale of 100 µm.

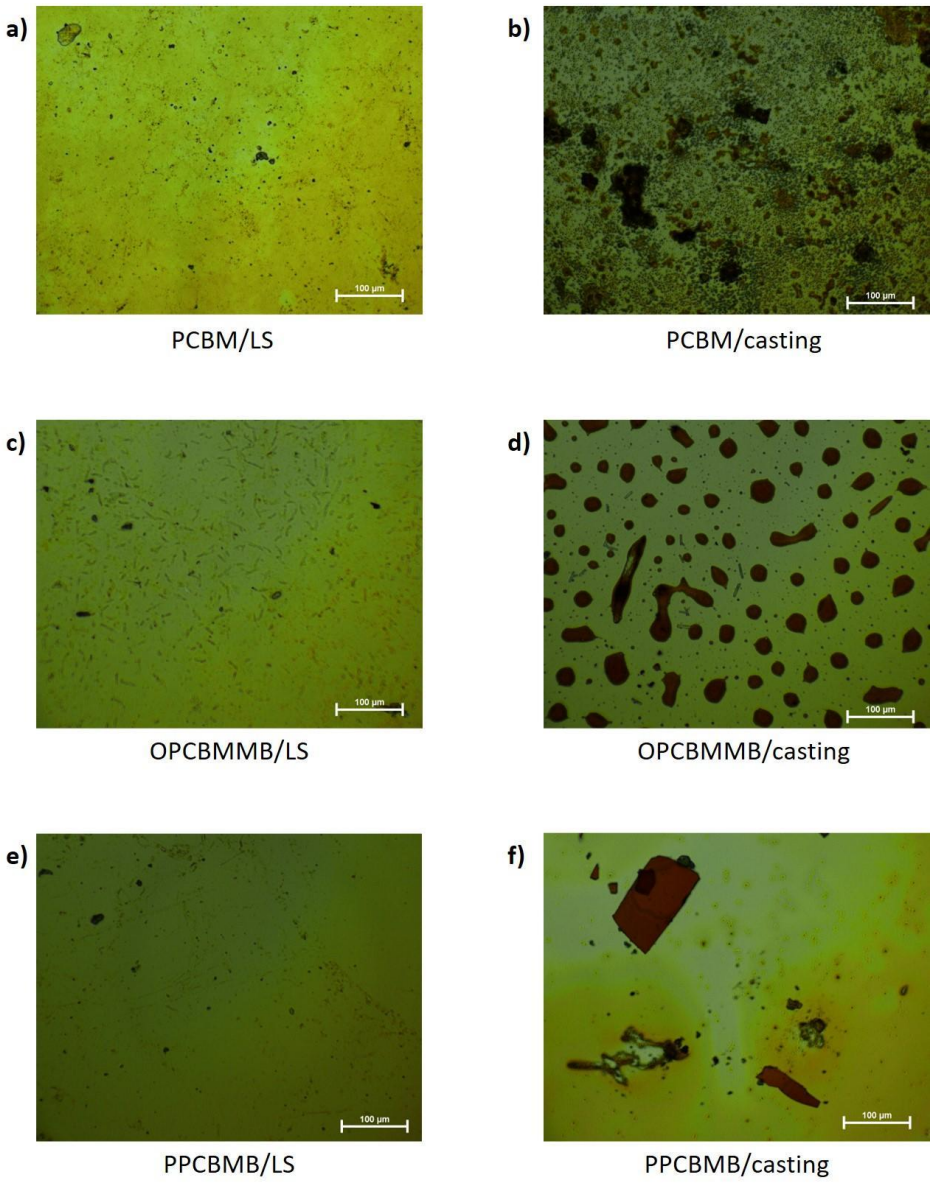

Figure 6. OM of: **a)** PCBM/LS; **b)** PCBM/cast; **c)** OPCBMMB/LS; **d) O**PCBMMB/cast; **e)** PPCBMB/LS; **f)** PPCBMB/cast. All images bar shows 100 µm.

With the optical microscopy images, we can observe that the LS films have more homogeneous surfaces, compared with the drop casting films. In the casting films, it is possible to see that the materials present different surface profiles from each other. We can see the presence of several aggregates on the surface of the PCBM film, however, smaller in size. Observing the OPCBMMB and PPCBMB films, it is possible to see the presence of less aggregates, but larger in size.

3.3 – UV-visible Optical Absorption Spectroscopy

Figure 7 shows the UV-visible absorption results obtained from the PCBM, OPCBMMB and PPCBMB thin films, deposited from Langmuir-Schaefer and drop casting techniques. One of the goals of UV-visible spectroscopy is to observe the linearity in the LS films growth, which guarantees the ordering and homogeneity of the film structure in each layer. In order to achieve this goal, the measurements in the LS films were performed during the deposition process, with 1, 3, 5, 9, 15 and 25 layers.

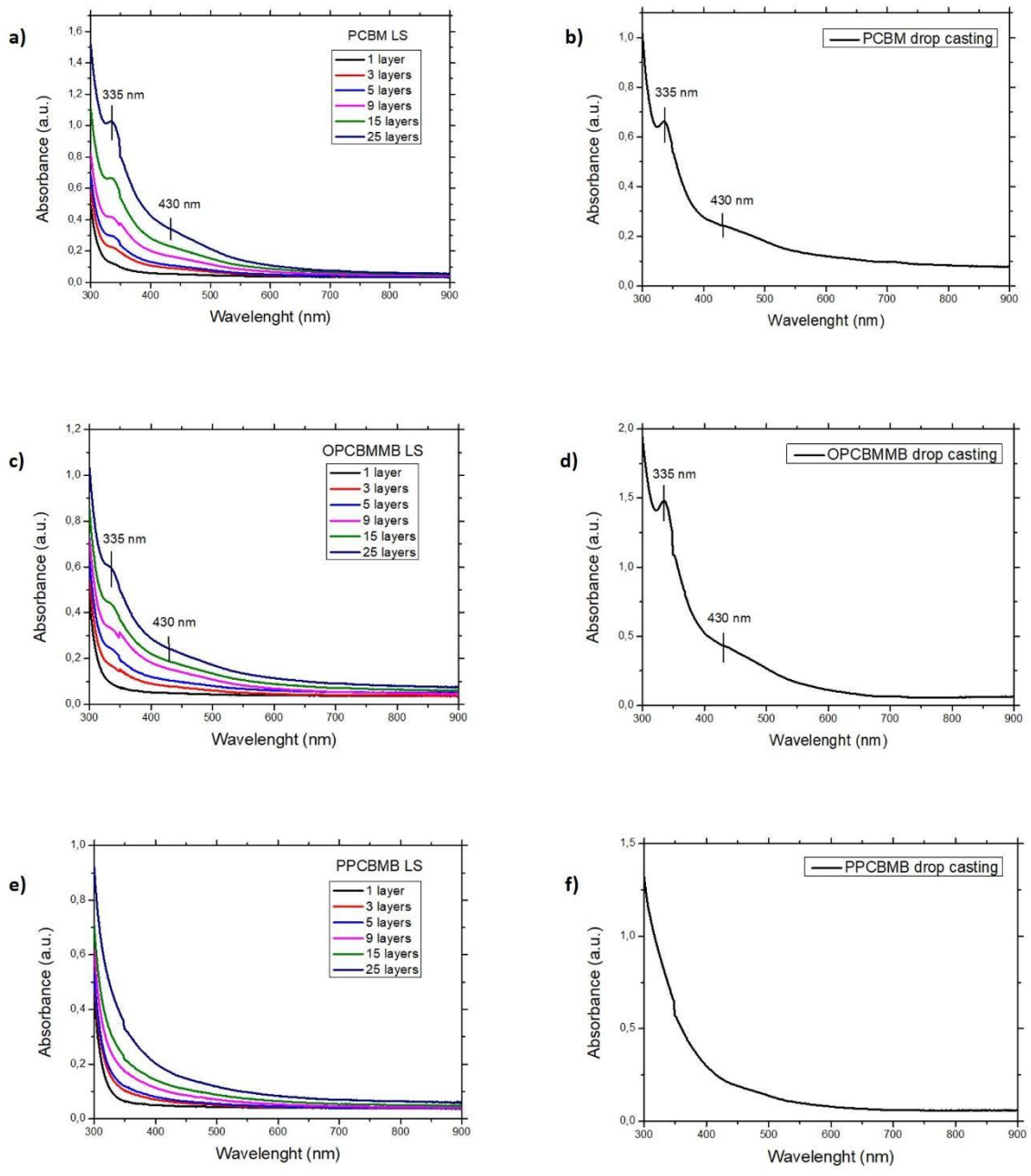

Figure 7. Optical absorption spectra of **a)** PCBM/LS; **b)** PCBM/casting; **c)** OPCBMMB/LS; **d) O**PCBMMB/casting; **e)** PPCBMB/LS; **f)** PPCBMB/casting

Analyzing the results obtained from the LS films, it is possible to see that the light absorption in these films happens in lower wavelengths, starting close to ultraviolet region, reaching an absorption peak in 335 nm, a characteristic behavior present on fullerenes, related to excited singlet transitions [44]. It is also possible to observe the presence of a discreet shoulder peak, around 430 nm, visible on PCBM and OPCBMMB spectra, corresponding to the fullerene bonds that connect their hexagonal structures [45], [46].

The similarity observed in both spectra, without the presence of a shift may indicate that both deposition techniques resulted in films with similar levels of structural organization. Although LS films in general tends to present a higher level of structural order, superior to drop casting films, the nature of fullerene to form aggregates in an uncontrolled manner may be preventing the formation of Langmuir films with the higher organization expected, since the functionalization employed in the fullerene presents different results in relation to the aggregation control [37].

In both deposition techniques, it is observed that PPCBMB, when compared to the other materials, has its most intense absorption region displaced to even lower wavelengths, in the ultraviolet region, caused by a reduction in the conjugation and symmetry in the fullerene, due to it synthetic process in which two additional double-bonds are broken [8], [47].

Analyzing the OPCBMMB absorption spectrum, it is observed that it presents a very similar result to the PCBM spectrum, indicating that the large amount of PCBM present in the OPCBMMB structure is able to mask most of the oligomer's electronic properties [7]. These similarities in both spectra also confirm, as found in earlier work, that the bonds formed during the synthesis process occurred at specific and symmetrical points in the fullerene spheres (1,4-phenylene), causing the material to maintain its initial symmetry [7], [48], [49].

Figure 8 presents the absorbance curves by layer number in the LS films of each material, taking as reference the wavelengths of 335 nm, corresponding to the absorption peaks for PCBM and OPCBMMB, and 430 nm for PPCBMB, where it is possible to

notice an increase in the absorbance intensity, which is directly proportional to the number of deposited layers, confirming that the films present a linear growth when deposited by the Langmuir-Schaefer technique.

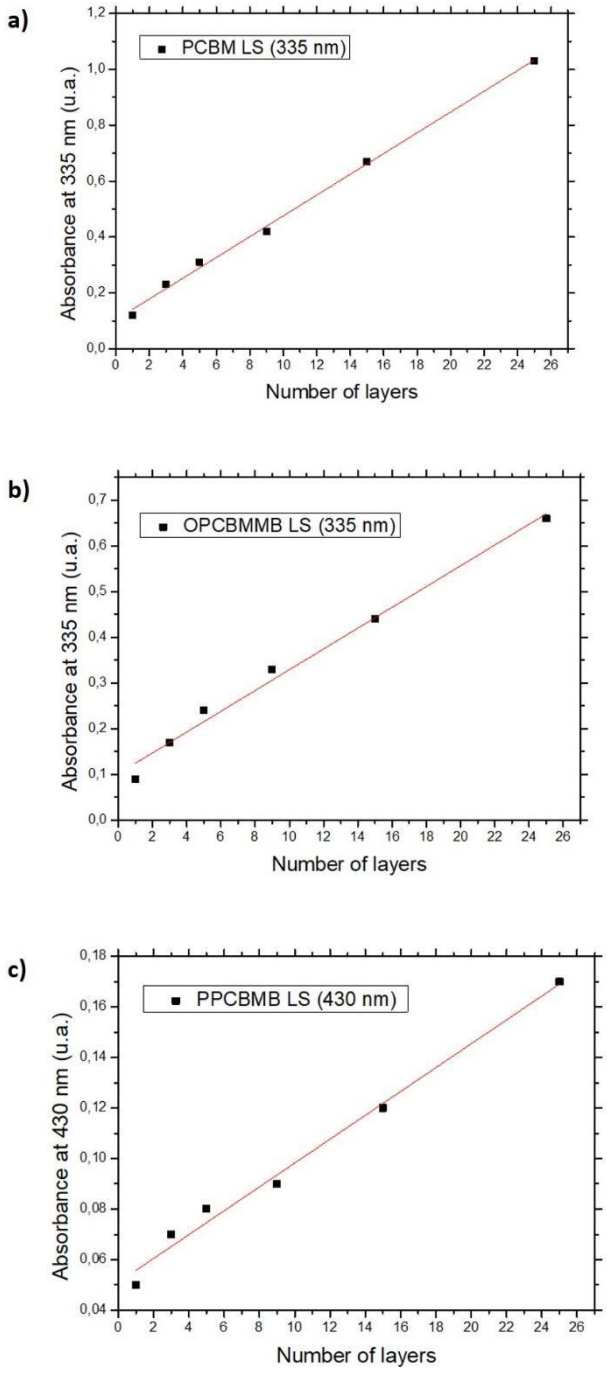

Figure 8. Relation between absorption and number of deposited layers of **a)** PCBM; **b)** OPCBMMB; **c)** PPCBMB.

3.4 – Electrical Characterizations in Direct Current

I versus V curves are shown in Figures 9 and 10, where we can observe that for both deposition techniques, the conductivity curve of PCBM is more accentuated in relation to the abscissa axis, when compared to OPCBMMB and PPCBMB.

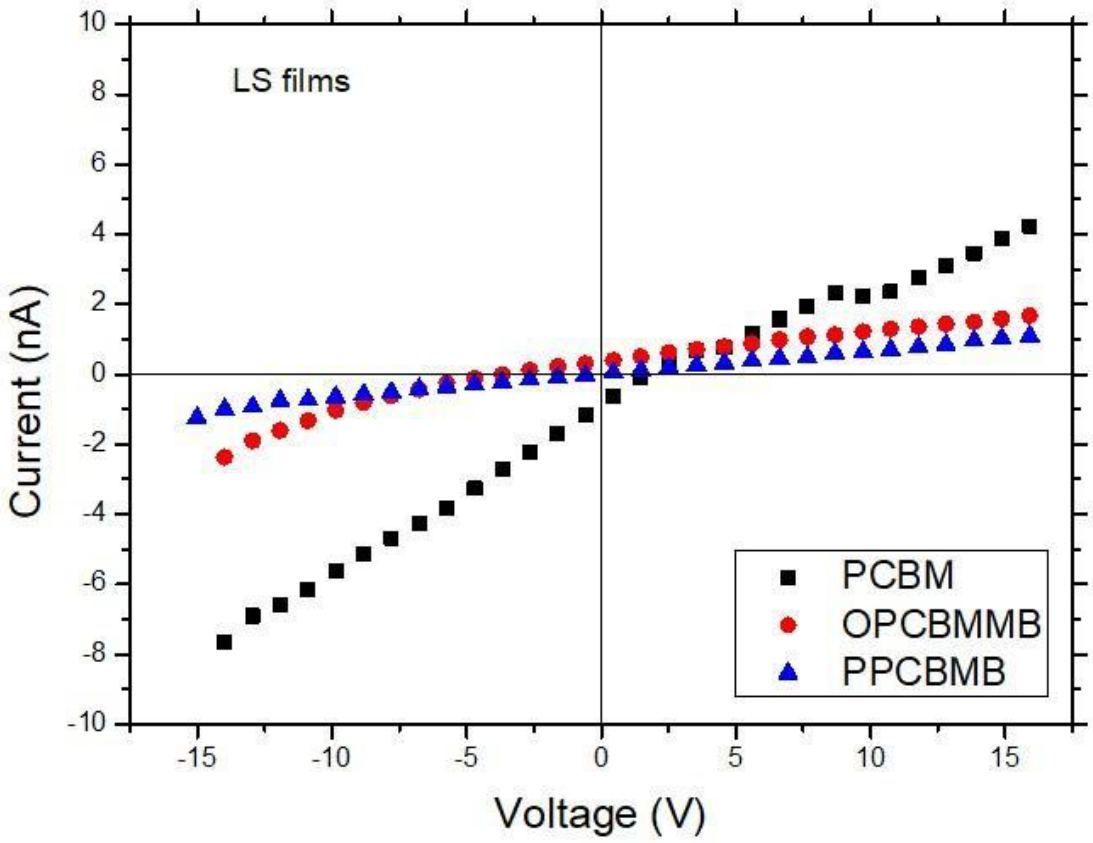

Figure 9. Current versus Voltage curves in the LS films of PCBM, OPCBMMB and PPCBMB.

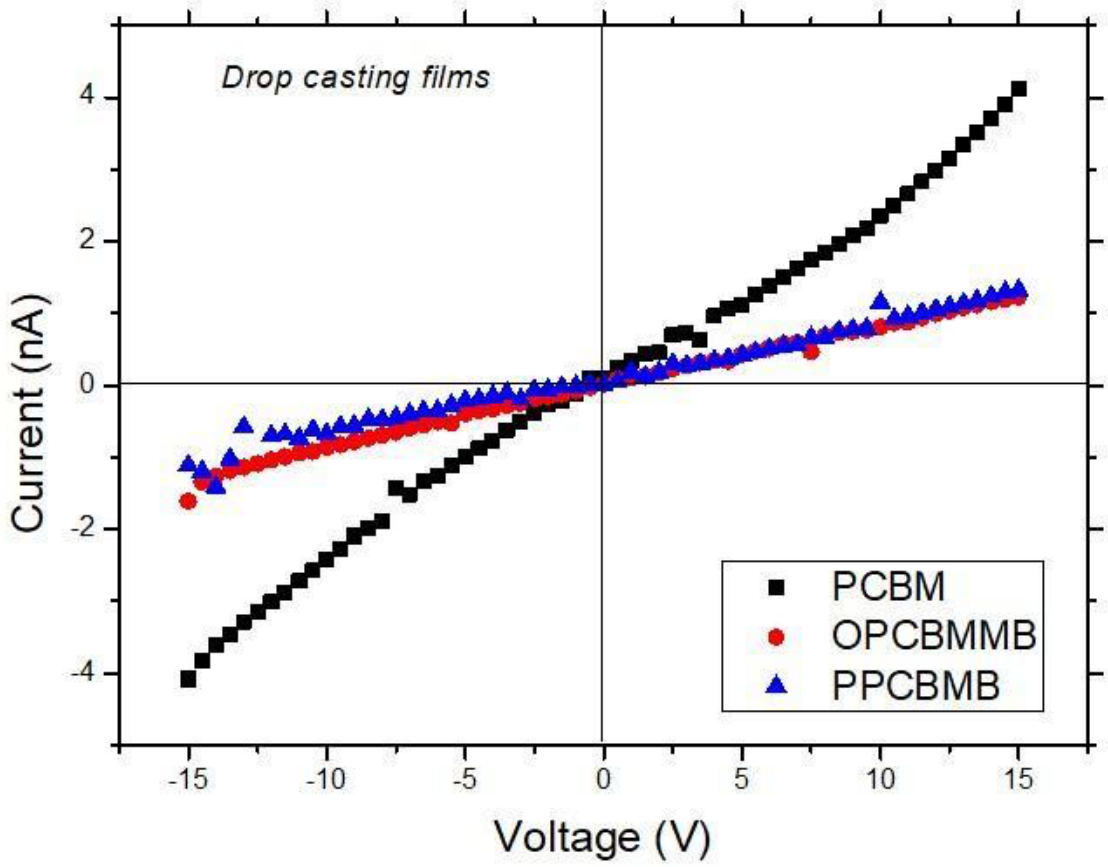

Figure 10. Current versus Voltage curves in the drop casting films of PCBM, OPCBMMB, and PPCBMB.

The linear plots obtained by *I versus V* curves show that the materials behave according to Ohm's Laws, varying linearly, due to the contact with an Au/film/Au configuration [50], especially in lower voltage regions. Ohmic contacts, such as those observed, have the characteristic of not influencing the carrier's density in the volume of the material when an electrical voltage is applied [50], [51]. This feature makes it possible calculate the electrical conductivity [52], as a linear equation of first degree ($y = ax + b$), with $b = 0$ can be used. From Ohm's Law, it is possible to determine the resistance (R) and the electrical conductivity (σ), since the conductivity is the inverse of the resistivity (ρ). Electrical resistance and conductivity values obtained for both deposition techniques are shown in Tables 3 and 4.

Table 3. Electrical resistance of PCBM, OPCBMMB and PPCBMB for the LS and drop casting films, obtained through the angular coefficient of the curves from Figures 1 and 2.

Resistance (Ω)	**Langmuir-Schaefer**	**Drop-cast**

PCBM	$2.53\ x\ 10^{9}$	$4.04\ x\ 10^{9}$
OPCBMMB	$8.56\ x\ 10^{9}$	$1.16\ x\ 10^{10}$
PPCBMB	$1.45\ x\ 10^{10}$	$1.03\ x\ 10^{10}$

Table 4. Electrical conductivity of PCBM, OPCBMMB and PPCCBMB for the LS and drop casting films.

Conductivity (S/m)	**Langmuir-Schaefer**	**Drop-cast**
PCBM	$2.01\ x\ 10^{-9}$	$1.26\ x\ 10^{-9}$
OPCBMMB	$5.96\ x\ 10^{-10}$	$4.38\ x\ 10^{-10}$
PPCBMB	$3.51\ x\ 10^{-10}$	$4.96\ x\ 10^{-10}$

In the studied materials, it is observed that the films produced by the Langmuir-Schaefer technique resulted, in general, in slightly higher values of electrical conductivity, compared to the drop-cast films, which would be expected from their greater molecular order, acting as a smoother path for the charges, compared to a film with less ordering in their structure.

This distinction can be described through the images obtained by AFM, where the surface mean roughness measurements showed that the surface of the LS films are slightly more homogeneous than drop-cast films, which contributes to charge transport in thin films, creating a smoother path for the charges [48], while the defects of a rough surface can create “traps” that imprison the charges via Poole-Frenkel effect [53], [54] and hinder their transport [26]–[28].

However, this does not occur in PPCBMB films, where the conductivity of the drop-cast films is slightly higher than the conductivity of the LS film, as well as observed in the AFM results, where the PPCBM LS films has a slightly rougher surface than the PPCBMB drop-cast film. The very dilute regime in which the polymers were deposited

in the Langmuir trough would tend to indicate that entanglement of the polymers would not be expected. However, they had very high molecular weights ($M_w \approx 73\ 800$ g mol^{-1}) which means it cannot be excluded as a possibility. Another possibility is oxidation of the fullerene in the air surrounding the film, which can give rise to ether linkages between chains. Just a few reactions can lead to quite large material changes, and this might explain the difference. Future work will look at using inert nitrogen atmospheres for Langmuir and casting.

3.5 – Electrical Characterization as NH_3 Sensors

The experiment was carried out on samples of both LS and drop casting thin films, in cycles of 10 minutes, alternating between the NH_3 atmosphere and the N_2 baseline. During the entire process, a constant voltage of 5 V was applied to the samples. The Current versus time (I vs. t) curves obtained are displayed on Figure 11.

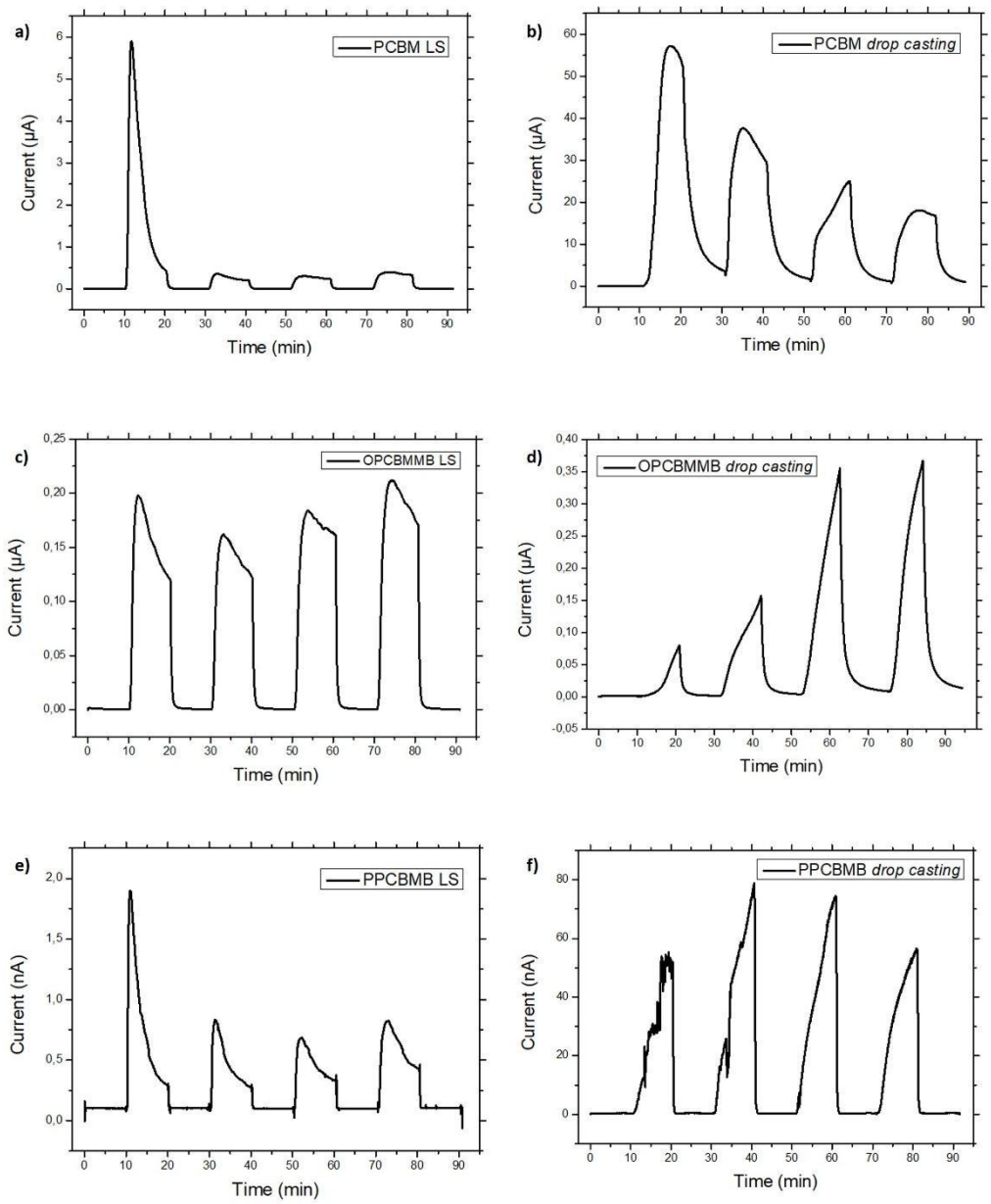

Figure 11. I vs. t NH_3 sensing measurements of **a)** PCBM/LS; **b)** PCBM/casting; **c)** OPCBMMB/LS; **d) O**PCBMMB/casting **e)** PPCBMB/LS; **f)** PPCBMB/casting.

The result show that the three materials exhibited electrical responses to passage of the NH_3 analyte, in both deposition techniques, resulting in a considerable increase in the measured electrical current, with emphasis on the LS films, which showed faster responses to the analyte stimulus, reaching the maximum of their responses in shorter times, in every measured cycle. This can also be related to the structural organization of the LS film, granting an easier path to the charge conduction.

The highest values obtained, however, occurred in the drop-cast films, where PCBM presented the highest peak of all samples, of 57 µA followed by OPCBMMB with a peak of 0.37 µA. Among the drop-cast films, the lowest peak was obtained from PPCBMB, with 78 nA. The LS films resulted in smaller peaks, with PCBM reaching a maximum of 5.9 µA, followed by OPCBMMB with a peak of 0.21 µA. Again, PPCBMB had the lowest peak, with 1.9 nA.

It is also observed that the materials exhibited different response profiles when exposed to the gas, so that in the LS films (Figure 11c), OPCBMMB presented a few intensity variations in the registered peaks, while PPCBMB (Figure 11e) presented a small drop from the second measured peak. PCBM (Figure 11a), on the other hand, presented a great decrease in intensity from the second peak. Although the current peaks stabilize starting from the second cycle in the PCBM LS film, the measured currents were very low, an issue observed in most of the samples studied. The measured current peaks are shown in Table 5.

Table 5. Current peaks registered on LS films during exposure to NH_3.

Current Peaks (LS)	1st peak	2nd peak	3rd peak	4th peak
PCBM	5.90 µA	0.36 µA	0.30 µA	0.39 µA
OPCBMMB	0.19 µA	0.16 µA	0.18 µA	0.21 µA
PPCBMB	1.90 nA	0.83 nA	0.68 nA	0.82 nA

In the drop-cast films, each material also presented a different response profile. PCBM (Figure 11b) showed a gradual decrease at each NH_3 cycle studied, while OPCBMMB (Figure 11d) showed the opposite behavior, with an increase in the current peak intensity, until reaching constant values. Between the drop-cast films, PPCBMB (Figure 11f) was the one that suffered the least variations in its current peaks, presenting similar current peak values at each cycle. The values of each current peak obtained in drop-cast films are shown in Table 6.

Table 6. Current peaks registered on drop casting films during exposure to NH_3.

Current Peaks (drop casting)	1st peak	2nd peak	3rd peak	4th peak
PCBM	57.2 µA	36.7 µA	28.9 µA	18.1 µA
OPCBMMB	0.08 µA	0.16 µA	0.36 µA	0.37 µA
PPCBMB	54.8 nA	78.8 nA	74.5 nA	56.4 nA

In all cases, it is observed that there was a quick response of the materials, in both techniques and in all cycles, with an immediate increase in the current, reaching their maximum intensity in few minutes. Additionally, at the end of the NH_3 cycles, the materials were capable of returning to the baseline current values (shown in Figures 9 and 10, at 5 V), showing that these processes are reversible.

The good performance observed in these materials when reacting to NH_3 can be explained due to the fact that they all have PCBM in common in their structures, since it is an n-type material (acceptor), which reacts favorably with NH_3, which is a p-type material (donor) [49], [50]. There is most likely a strong nucleophilic attraction from the nitrogen's electron lone pair orbital with the highly electrophilic fullerene, where the materials capture the gas charges, which start to act in the charge conduction process [55], [56]. This would also explain why the drop casting films showed a higher response, since the technique tends to create a less homogeneous surface, able to trap NH_3 molecules between their aggregates, favoring the capture of charges to participate in the conduction process [28], [57].

This can be related to the AFM images of the thin films (Figure 5, Table 2), where the results showed that the PCBM drop-cast films presented a rougher surface, with the presence of several agglomerates compared to the PCBM LS film, which presented a more homogeneous and less rough surface. This translates to the results from the gas measurements, where the drop-cast films, which are rougher, obtained more intense current peaks in the presence of the analyte. The region where the conduction process happens is dictated by the electrode's geometrical characteristics, with the electric field

being applied horizontally between the digits, which means that the conduction happens only between the 110 nm thickness of the electrode and the charges above this ideally should not participate this process. This means that the thickness of the film must be enough to cover the electrodes, but anything above the electrode, ideally doesn't contribute to the conduction process.

In contrast, OPCBMMB and PPCBMB films showed similar roughness values for both deposition techniques, due to their greater polymeric nature being more determinate in their film formation [37]. This also translates into the results obtained in the gas measurements, with the OPCBMMB and PPCBMB films of both techniques showing a smaller difference between the current peak values in the presence of NH_3.

The large drop observed in both PCBM films can occur due to a possible nucleophilic reaction of the analyte with the material, reducing its ability to exchange electrical charges, which translates into the less intense peaks observed [5]. The absence of these drops in the current values in the other materials indicates that the branches present in the structure of OPCBMMB and PPCBMB are able to block the permanent reaction with the NH_3 gas, which reduces the interactions with ammonia, resulting in smaller peaks, but allows a better reproducibility over the observed cycles.

Observing Figure 11, the results of the I vs. t ammonia measurements show that not only did the materials respond favorably to the interaction with NH_3 gas, but also that the answers are possible to be reproduce, corroborating with the idea to use PCBM, OPCBMMB and PPCBMB as an active layer in the production of NH_3 gas sensor that can be reused [58], [59]. Highlighting the OPCBMMB LS film, which, in addition to showing little variation between the current peaks measured in each cycle, also obtained faster answers than the drop-cast films.

4. CONCLUSION

In this work, the manufacture of PCBM, OPCBMMB and PPCBMB thin films is described using the Langmuir-Schaefer and drop casting techniques, in order to perform their characterization and verify their applicability as an ammonia sensor. The results obtained with UV-vis absorption measurements showed the linear growth of the Langmuir films, with absorption peaks at 335 nm, characteristic of fullerenes. AFM and optical microscopy results showed the formation of numerous aggregates in the drop casting films, while the Langmuir-Schaefer films showed greater surface homogeneity. Gas measurements shoed that all materials respond to ammonia stimulation, due to the donor nature of the analyte and the acceptor nature of the materials studied. Despite showing results with greater reproducibility, the current values in the peaks observed in the OPCBMMB and PPCBMB films were much lower than the peaks obtained in the PCBM films, in both deposition techniques. This implies that, even with good reproducibility, current variations would require a very sensitive voltage source to detect them. Furthermore, discarding the first cycle in the PCBM films, the remaining cycles show a good reproducibility.

REFERENCES

[1] H. W. Kroto, J. R. Heath, S. C. O'Brien, R. F. Curl, and R. E. Smalley, "C60: Buckminsterfullerene," *Nature*, vol. 318, pp. 162–163, 1985.

[2] F. Wudl, "Fullerene materials," *Journal of Materials Chemistry*, vol. 12, no. 7. pp. 1959–1963, 2002. doi: 10.1039/b201196d.

[3] H. W. Kroto, "C60 buckminsterfullerene, other fullerenes and the icospiral shell," *Comput. Math. with Appl.*, vol. 17, no. 1–3, pp. 417–423, 1989, doi: 10.1016/0898-1221(89)90171-5.

[4] M. A. Wilson, L. S. K. Pang, G. D. Willett, K. J. Fisher, and I. G. Dance, "FULLERENES-PREPARATION, PROPERTIES, AND CARBON CHEMISTRY," 1992.

[5] G. P. Miller, "Reactions between aliphatic amines and [60]fullerene: a review," *Comptes Rendus Chimie*, vol. 9, no. 7–8. pp. 952–959, Jul. 2006. doi: 10.1016/j.crci.2005.11.020.

[6] H. C. Wong *et al.*, "Morphological stability and performance of polymer-fullerene solar cells under thermal stress: The impact of photoinduced PC60BM oligomerization," *ACS Nano*, vol. 8, no. 2, pp. 1297–1308, 2014, doi: 10.1021/nn404687s.

[7] H. H. Ramanitra *et al.*, "Increased thermal stabilization of polymer photovoltaic cells with oligomeric PCBM," *J. Mater. Chem. C*, vol. 4, no. 34, pp. 8121–8129, 2016, doi: 10.1039/c6tc03290g.

[8] M. Stephen *et al.*, "Sterically controlled azomethine ylide cycloaddition polymerization of phenyl-C61-butyric acid methyl ester," *Chem. Commun.*, vol. 52, no. 36, pp. 6107–6110, 2016, doi: 10.1039/c6cc01380e.

[9] J. A. Zasadzinski, R. Viswanthan, L. Madsen, J. Garnaes, and D. K. Schwartz, "Langmuir-Blodgett Films," *Science (80-.).*, vol. 263, no. 5154, pp. 1726–1733, 1994.

[10] V. J. R. de Oliveira, M. S. Borro, L. Rubim do Monte Jesus, M. L. Braunger, and C. de A. Olivati, "Using Langmuir-Schaefer deposition technique to improve the gas sensing performance of regiorandom polythiophene films," *Sensors and Actuators Reports*, vol. 4, p. 100094, Nov. 2022, doi: 10.1016/j.snr.2022.100094.

[11] M. Ito *et al.*, "Hyper 100 °C Langmuir–Blodgett (Langmuir–Schaefer) Technique for Organized Ultrathin Film of Polymeric Semiconductors," *Langmuir*, vol. 38, no. 17, pp. 5237–5247, May 2022, doi: 10.1021/acs.langmuir.1c02596.

[12] C. P. L. Rubinger *et al.*, "Langmuir–Blodgett and Langmuir–Schaefer films of poly(5-amino-1-naphthol) conjugated polymer," *Appl. Surf. Sci.*, vol. 253, no. 2, pp. 543–548, Nov. 2006, doi: 10.1016/j.apsusc.2005.12.096.

[13] K. C. Persaud, "Polymers for chemical sensing," *Mater. Today*, vol. 8, no. 4, pp. 38–44, Apr. 2005, doi: 10.1016/S1369-7021(05)00793-5.

[14] Pedro Henrique Suman, "Caracterizção de nanoestruturas de óxido de estanho como sensores de gás," UNIVERSIDADE ESTADUAL PAULISTA "Júlio de Mesquita Filho," Araraquara, 2012.

[15] F. Aliyu and T. Sheltami, “Development of an energy-harvesting toxic and combustible gas sensor for oil and gas industries,” *Sensors Actuators, B Chem.*, vol. 231, pp. 265–275, 2016, doi: 10.1016/j.snb.2016.03.037.

[16] G. Velasco and J. P. Schnell, “Gas sensors and their applications in the automotive industry,” *J. Phys. E.*, vol. 16, no. 10, pp. 973–977, 1983, doi: 10.1088/0022-3735/16/10/006.

[17] B. Bourrounet, T. Talou, and A. Gaset, “Application of a multi-gas-sensor device in the meat industry for boar-taint detection,” *Sensors Actuators B. Chem.*, vol. 27, no. 1–3, pp. 250–254, 1995, doi: 10.1016/0925-4005(94)01596-A.

[18] J. Fraden and J. G. King, “Handbook of Modern Sensors: Physics, Designs, and Applications, 2nd ed.,” *Am. J. Phys.*, vol. 66, no. 4, pp. 357–359, Apr. 1998, doi: 10.1119/1.18801.

[19] S. V. Krupa, “Effects of atmospheric ammonia (NH3) on terrestrial vegetation: A review,” *Environmental Pollution*, vol. 124, no. 2. Elsevier Ltd, pp. 179–221, 2003. doi: 10.1016/S0269-7491(02)00434-7.

[20] I. Trebs, F. X. Meixner, J. Slanina, R. Otjes, P. Jongejan, and M. O. Andreae, “Atmospheric Chemistry and Physics Real-time measurements of ammonia, acidic trace gases and water-soluble inorganic aerosol species at a rural site in the Amazon Basin,” 2004. [Online]. Available: www.atmos-chem-phys.org/acp/4/967/

[21] J.-F. Tang, C.-C. Fang, and C.-L. Hsu, “Enhanced organic gas sensor based on Cerium- and Au-doped ZnO nanowires via low temperature one-pot synthesis,” *Appl. Surf. Sci.*, vol. 613, p. 156094, Mar. 2023, doi: 10.1016/j.apsusc.2022.156094.

[22] C. A. Betty, S. Choudhury, and A. Shah, “Nanostructured metal oxide semiconductors and composites for reliable trace gas sensing at room temperature,” *Surfaces and Interfaces*, vol. 36, p. 102560, Feb. 2023, doi: 10.1016/j.surfin.2022.102560.

[23] H. Du, X. Maimaitiyiming, Y. Luo, and A. Obolda, “A highly sensitive ammonia gas sensor based on non-covalent functionalized single-walled carbon nanotubes with Schiff Base polyphenylene polymer,” *Sensors Actuators B Chem.*, vol. 394, p. 134426, Nov. 2023, doi: 10.1016/j.snb.2023.134426.

[24] Z. Shahrbabaki *et al.*, “A Flexible and Polymer-Based Chemiresistive CO 2 Gas Sensor at Room Temperature,” *Adv. Mater. Technol.*, vol. 8, no. 10, May 2023, doi: 10.1002/admt.202201510.

[25] N. F. Sheppard, R. C. Tucker, and C. Wu, “Electrical Conductivity Measurements Using Microfabricated Interdigitated Electrodes,” *Anal. Chem.*, vol. 65, no. 9, pp. 1199–1202, 1993, doi: 10.1021/ac00057a016.

[26] L. C. Pimentel, “Filmes Finos Multicamadas De Polímeros Condutores, Nanotubos De Carbono E Fulerenos Modificados Para Aplicação Na Conversão De Energia Solar,” 2012.

[27] S. V. F. DE CASTRO, “Sensor voltamétrico para detecção de trinitrotolueno baseado em nanocompósito de óxido de grafeno reduzido e nanotubos de

carbono," vol. 2021, no. 11, p. 7162, Aug. 2012, doi: 10.14393/ufu.di.2018.1192.

[28] O. Kanoun *et al.*, "Flexible carbon nanotube films for high performance strain sensors," *Sensors (Switzerland)*, vol. 14, no. 6. Molecular Diversity Preservation International, pp. 10042–10071, Jun. 06, 2014. doi: 10.3390/s140610042.

[29] A. V. S. Simõis *et al.*, "Polyfullerene Thin Films Applied as NH3 Sensors," *Mater. Res.*, vol. 24, 2021, doi: 10.1590/1980-5373-MR-2021-0435.

[30] A. Kaliyaraj Selva Kumar, Y. Zhang, D. Li, and R. G. Compton, "A mini-review: How reliable is the drop casting technique?," *Electrochemistry Communications*, vol. 121. Elsevier Inc., Dec. 01, 2020. doi: 10.1016/j.elecom.2020.106867.

[31] L. M. Blinov, "Langmuir films," *Sov. Phys. - Uspekhi*, vol. 31, no. 7, pp. 623–644, 1988, doi: 10.1070/PU1988v031n07ABEH003573.

[32] T. A. de Assis *et al.*, "Effect of the local morphology in the field emission properties of conducting polymer surfaces," *J. Phys. Condens. Matter*, vol. 25, no. 28, p. 285106, Jul. 2013, doi: 10.1088/0953-8984/25/28/285106.

[33] E. Assunção Da Silva, "EFEITO DA ADIÇÃO DE MOLÉCULAS ANFIFÍLICAS NA FORMAÇÃO DE FILMES LANGMUIR E LANGMUIR-BLODGETT DE DERIVADOS ALQUILADOS DO POLITIOFENO: APLICAÇÃO EM SENSORES," UNIVERSIDADE ESTADUAL PAULISTA "JÚLIO DE MESQUITA FILHO," Presidente Prudente, 2014.

[34] S. Fabiano, S. Braun, M. Fahlman, X. Crispin, and M. Berggren, "Effect of gate electrode work-function on source charge injection in electrolyte-gated organic field-effect transistors," *Adv. Funct. Mater.*, vol. 24, no. 5, pp. 695–700, Feb. 2014, doi: 10.1002/adfm.201302070.

[35] W. Olthuis, W. Streekstra, and P. Bergveld, "Theoretical and experimental determination of cell constants of planar-interdigitated electrolyte conductivity sensors," *Sensors Actuators B. Chem.*, vol. 24, no. 1–3, pp. 252–256, 1995, doi: 10.1016/0925-4005(95)85053-8.

[36] M. Ferreira, W. Caetano, R. Itri, M. Tabak, and O. N. Oliveira, "Técnicas de caracterização para investigar interações no nível molecular em filmes de Langmuir e Langmuir-Blodgett (LB)," *Quim. Nova*, vol. 28, no. 3, pp. 502–510, 2005, doi: 10.1590/S0100-40422005000300024.

[37] S. Ravaine, C. Mingotaud, and P. Delhaès, "Langmuir and Langmuir-Blodgett films of C60 derivatives," *Thin Solid Films*, vol. 284–285, pp. 76–79, 1996, doi: 10.1016/S0040-6090(95)08275-1.

[38] C. Long, Y. Xu, C. Zhu, and D. Zhu, "TEM STUDY ON LANGMUIR-BLODGETT FILMS OF TWO NOVEL C, DERIVATIVES," 1997.

[39] D. Felder-Flesch, "Self- Or induced organization of [60]fullerene hexakisadducts," *Struct. Bond.*, vol. 159, pp. 101–144, Jun. 2013, doi: 10.1007/430_2013_111.

[40] L. K. M. Roncaselli *et al.*, "Influence of solvents on the morphology of Langmuir and Langmuir-Schaefer films of PCBM and PCBM-based oligomers and polymers," *Phys. Chem. Chem. Phys.*, vol. 24, no. 20, pp. 12442–12456, 2022, doi: 10.1039/d1cp05408b.

[41] V. Oliveira, E. Silva, and C. Olivati, “Fabricação e caracterização de filmes finos de OC8OC8-PPV aplicados em dispositivos sensores de umidade,” *J. Exp. Tech. Instrum.*, vol. 1, no. 1, pp. 27–40, Mar. 2018, doi: 10.30609/jeti.2018-1.5270.

[42] L. K. M. Roncaselli, “ESTUDO E CARACTERIZAÇÃO DE FILMES NANOESTRURADOS DE DERIVADOS DE POLI-FULERENOS,” UNESP, Faculdade de Ciências e Tecnologia, Presidente Prudente, 2021.

[43] C. C. H. No, D. Zhou, L. Gan, C. Luo, H. Tan, and C. Huang, “Langmuir - Blodgett Films and Photophysical Properties of a C 60 - Sarcosine Methyl Ester,” vol. 60, no. 2, pp. 3150–3156, 1996.

[44] S. Cook, R. Katoh, and A. Furube, “Ultrafast studies of charge generation in PCBM: P3HT blend films following excitation of the fullerene PCBM,” *J. Phys. Chem. C*, vol. 113, no. 6, pp. 2547–2552, Feb. 2009, doi: 10.1021/jp8050774.

[45] R. C. Hiorns *et al.*, “Synthesis of donor-acceptor multiblock copolymers incorporating fullerene backbone repeat units,” *Macromolecules*, vol. 43, no. 14, pp. 6033–6044, Jul. 2010, doi: 10.1021/ma100694y.

[46] S. Miki, M. Kitao, and K. Fukunishi, “Introduction of two benzyl groups to C60 by using the Collman reagent,” *Tetrahedron Lett.*, vol. 37, no. 12, pp. 2049–2052, 1996, doi: 10.1016/0040-4039(96)00215-8.

[47] P. Hare *et al.*, “Electronic Spectra and Transitions of the Fullerene C60,” *Chem. Phys.*, vol. 160, pp. 451–466, 1992.

[48] M. Schnell, “Understanding high-resolution spectra of nonrigid molecules using group theory,” *ChemPhysChem*, vol. 11, no. 4, pp. 758–780, 2010, doi: 10.1002/cphc.200900760.

[49] J. Liu, X. Guo, Y. Qin, S. Liang, Z. X. Guo, and Y. Li, “Dumb-belled PCBM derivative with better photovoltaic performance,” *J. Mater. Chem.*, vol. 22, no. 5, pp. 1758–1761, Feb. 2012, doi: 10.1039/c2jm15322j.

[50] H. Iwai, S. M. Sze, Y. Taur, and H. Wong, *Physics of Semiconductor Devices*, Third Edit. Chichester, UK: John Wiley & Sons, Ltd, 2013. doi: 10.1002/9781118517543.ch2.

[51] H. Tomozawa, D. Braun, S. Phillips, R. Worland, A. Heeger, and H. Kroemer, “Metal-polymer Schottky barriers on processible polymers,” *Synth. Met.*, vol. 28, no. 1–2, pp. 687–690, Jan. 1989, doi: 10.1016/0379-6779(89)90591-2.

[52] C. K. Chiang *et al.*, “Electrical conductivity in doped polyacetylene,” *Phys. Rev. Lett.*, vol. 39, no. 17, pp. 1098–1101, Oct. 1977, doi: 10.1103/PhysRevLett.39.1098.

[53] J. Urbančič *et al.*, “Time-of-flight photoconductivity investigation of high charge carrier mobility in Ti3C2Tx MXenes thin-film,” *Diam. Relat. Mater.*, vol. 135, p. 109879, May 2023, doi: 10.1016/j.diamond.2023.109879.

[54] X. Lin, J. Jin, J. Kim, Q. Xin, J. Zhang, and A. Song, “Effects of gate roughness on low voltage InGaZnO thin-film transistors with ultra-thin anodized Al x O y dielectrics,” *Semicond. Sci. Technol.*, vol. 38, no. 3, p. 035023, Mar. 2023, doi: 10.1088/1361-6641/acba3e.

[55] C. Kumar, G. Rawat, H. Kumar, Y. Kumar, R. Prakash, and S. Jit, “Electrical and ammonia gas sensing properties of poly (3, 3‴- dialkylquaterthiophene) based organic thin film transistors fabricated by floating-film transfer method,” *Org. Electron.*, vol. 48, pp. 53–60, Sep. 2017, doi: 10.1016/j.orgel.2017.05.040.

[56] C. Kumar *et al.*, “Electrical and ammonia gas sensing properties of PQT-12/CdSe quantum dots composite-based organic thin film transistors,” *IEEE Sens. J.*, vol. 18, no. 15, pp. 6085–6091, Aug. 2018, doi: 10.1109/JSEN.2018.2845873.

[57] Yuyan Chen *et al.*, “[6,6]-Phenyl C61 butyric acid methyl ester/α-sexithiophene hetero-junction thin film transistors gas sensors for ammonia detection,” in *2015 IEEE SENSORS*, IEEE, Nov. 2015, pp. 1–4. doi: 10.1109/ICSENS.2015.7370577.

[58] M. S. Park, A. A. Meresa, C. M. Kwon, and F. S. Kim, “Selective wet-etching of polymer/fullerene blend films for surface- and nanoscale morphology-controlled organic transistors and sensitivity-enhanced gas sensors,” *Polymers (Basel).*, vol. 11, no. 10, Oct. 2019, doi: 10.3390/polym11101682.

[59] H. L. Cheng, W. Q. Lin, and F. C. Wu, “Effects of solvents and vacancies on the electrical hysteresis characteristics in regioregular poly(3-hexylthiophene) organic thin-film transistors,” *Appl. Phys. Lett.*, vol. 94, no. 22, 2009, doi: 10.1063/1.3148332.